

Nuclear point mass effects in the interaction of energetic ion with carbon nanotubes

Li-Ping Zheng¹ · Long Yan¹ · Zhi-Yong Zhu¹ · Guo-Liang Ma¹

Received: 13 July 2015 / Accepted: 26 January 2016 / Published online: 1 March 2016
© Springer-Verlag Berlin Heidelberg 2016

Abstract We have calculated deposited energies of various energetic ions in carbon nanotubes, to study nuclear point mass effects, with the help of a static Monte Carlo (MC) simulation program. As a result of nuclear point mass effects, we show that at the same incident energy, the ion-deposited energy maximizes, while its mass has intermediate mass values, such as ¹¹B, ¹²C and ¹⁴N ion masses, under hundreds keV ⁴He, ¹¹B, ¹²C, ¹⁴N, ²⁰Ne, ²⁸Si and ⁴⁰Ar ion irradiations of a thin-walled carbon nanotube. We also show that at the same incident energy, the coordination defect number maximizes, while its mass has an intermediate mass (²⁰Ne) value, under hundreds keV ⁴He, ²⁰Ne and ⁴⁰Ar ion irradiations of the thin-walled nanotube. We derive an ion-deposited energy formula to analyze these maximum phenomena, and compare the MC simulation results with the MD (molecular dynamics) ones.

1 Introduction

In energetic (\leq MeV) particle collision fields, stopping can be distinguished into two kinds, i.e., nuclear stopping and electronic stopping [1–23]. Electronic stopping of charged particles in matter is known to be rather insensitive to specific properties of the stopping material [2]. In particle penetration and radiation effect theories, Sigmund clarifies general aspects and stopping of swift point charges [1]. Evidently, according to his theories, the well-known $4Mm/(M+m)^2$ effects may belong to the nuclear point mass

effects. Here, M and m are ion and atom masses. Based on the conservation of transverse energy and that of transverse momentum, the $4Mm/(M+m)^2$ effects mean each collision between one and another point mass particles along a straight line, if one and another point masses equal M and m , respectively. In our opinion, his theories exhibit two foundational effects, i.e., the nuclear point charge effects and the nuclear point mass effects. The nuclear point mass effects are independent of the interaction potentials produced by nuclear point charges, such as the $4Mm/(M+m)^2$ effects suggested by us, but the nuclear point charge effects depend on the interaction potentials, such as the cross-sectional σ effects suggested by Krasheninnikov et al. [$\sigma = \pi p^2$, where p is the impact parameter (Fig. 5)].

The interaction of energetic ions with carbon nanotubes plays a fundamental role both in the field of ion beam irradiation and in nanoscience. To understand the basic physics of damage creation and stopping ions of different types, it is instructive to dwell first upon the irradiation of single-walled carbon nanotubes (SWCNTs) due to their simple and well-defined structure, between SWCNTs and MWCNTs (multi-walled carbon nanotubes). Molecular dynamics (MD) simulation works [7–11] have studied this interaction up to keV ion-irradiation energies. For stopping studies, reasoning from the data on He, Ne, Ar, Kr and Xe ion irradiations of SWCNTs and MWCNTs, it is clear that only the latter could be used to effectively stop keV ions. Further, MWCNTs with tens of the graphitic shells can easily stop energetic ions with energies up to 10 keV. For damage studies, the MD simulations find the irradiation-induced damage which proved to be higher for heavy ions than for light ones due to higher values of the cross section for the defect production in the SWCNT or the MWCNT [23].

In the MD simulations of the energetic-ion-induced coordination defects from light to heavy ions, in the

✉ Guo-Liang Ma
glma@sinap.ac.cn

¹ Shanghai Institute of Applied Physics, Chinese Academy of Sciences, P.O. Box 800-204, Shanghai 201800, China

SWCNT or the MWCNT, there is no discussion about experimental data to validate the modeling [7–11]. H, C, N, Si and Ar ion beam irradiations are usually thought to induce defects and disordered structures in materials and then to destroy the properties of the materials. However, our recent experiments [24–26] about the ion beam irradiations on the carbon nanotubes (CNTs) have indicated that the ion beam modification mechanism of CNTs is completely different from traditional one of bulk materials, and ion beam irradiations can lead to self-organized structures in CNTs, such as amorphous junctions and CNT junctions. Moreover, the irradiated CNTs exhibit an improved conductivity and an enhanced field emission. To our knowledge, no experiments have measured the energetic-ion mass effects on tube damage, until now.

The MC simulations and the MD simulations have different superiorities. The MC simulations use binary-interaction potentials and computational cells with infinite atoms. However, the MD simulations use multiple-interaction potentials and computational cells with limited atoms, so they are necessary to suppose boundary conditions. In the MD simulations, the energetic-ion collision with atoms primarily comes from a collision contribution between the ion and the first neighbor atom, while the ion should approach the first one. Such a collision contribution means the classical approach. For the interaction of energetic ions with the MWCNT (or SWCNT), in the MC simulations, the tube is infinite long; but in the MD simulations, usual periodic boundary conditions are supposed along tube-axis direction. By the way, it is noteworthy that channeling was primarily discovered as a result of computer simulations of ion beam propagation along atomic rows in a crystal, based on binary collisions of ions with atoms [3].

It is clearly known that the ion-deposited energy plays an important role in radiation damage and stopping mechanisms. Therefore, for better understanding of these mechanisms [2, 7–23], it might be informative that we calculate the deposited energies of various energetic ions, especially at incident energies up to hundreds keV. This is the main goal of our present simulation works.

The present static MC simulation programs include the first and the second steps (Sect. 2). At the first step, we not only calculate ion-deposited energies but also record broken atomic bond, Frenkel pair, stopped ion and stopped recoil atom positions, in the MWCNT (or SWCNT). At the second step, we calculate the coordination defects and use a Kinchin–Pease model to estimate the number of vacancies produced in the MWCNT (or SWCNT). Therefore, we can describe the carbon nanotubes how to be disordered. Under hundreds keV ion irradiations, at the first step, we find that the hundreds keV incident ion easily and swiftly penetrates through the thin-walled carbon nanotube while

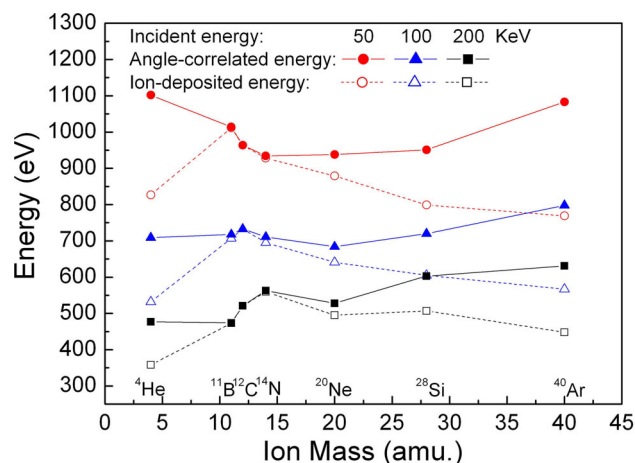


Fig. 1 Average ion-deposited energy $E_0 - E_{\text{penetrating}}$ (open) and the average angle-correlated energy $\sum_{i=0}^{n-1} E_i \sin^2(\theta_{i+1}/2)$ (solid) as functions of the ion mass for ${}^4\text{He}$, ${}^{11}\text{B}$, ${}^{12}\text{C}$, ${}^{14}\text{N}$, ${}^{20}\text{Ne}$, ${}^{28}\text{Si}$ and ${}^{40}\text{Ar}$ ion irradiations of a MWCNT composed of (10,10), (15,15) and (20,20) SWCNTs, at 50 (circles), 100 (triangles) and 200 keV (squares) incident energies. Here, $\sum_{i=0}^{n-1} E_i \sin^2(\theta_{i+1}/2)$ comes from formula (7)

in this tube, the ion-deposited energy is much less than, i.e., \ll , its incident energy. We also find that the $4Mm/(M+m)^2$ effects dominate the ion-deposited energies (Figs. 1, 3). At the second step, we find that the $4Mm/(M+m)^2$ effects dominate coordination defects and vacancies (Sect. 5).

2 MC simulation program series

Our Monte Carlo (MC) simulation program series has been employed in investigating particle motions exclusively along a straight-line segment in amorphous and crystalline [12, 19, 20, 22] materials. The present static MC simulation program utilizes a binary collision model [2, 12–22] based on the Moliere potential for the ion–atom (or atom–atom) interaction and on the continuously slowing approximation for electronic stopping, at low temperatures. Carbon nanotubes (the MWCNT) in a super-lattice are kept in a position of equilibrium by van der Waals forces, and the gap between the walls of neighboring nanotubes is usually ~ 0.315 nm. The thermal vibration is modeled by giving each lattice atom a random displacement (commonly below 0.01 nm).

Our recent static MC simulation works have studied isotopic mass effects for energetic-ion channeling in the SWCNT [12]. In our present static MC simulation works, ${}^4\text{He}$, ${}^{11}\text{B}$, ${}^{12}\text{C}$, ${}^{14}\text{N}$, ${}^{20}\text{Ne}$, ${}^{28}\text{Si}$ and ${}^{40}\text{Ar}$ ion beams normally irradiate the (20, 20) SWCNT or the MWCNT composed of (10, 10), (15, 15) and (20, 20) SWCNTs, at incident energies $E_0 \geq 50$ keV. The MWCNT is infinite long

because of atomic-number-infinite computational cells, and the incident beam size equals the outer diameter of the (20, 20) SWCNT. For the given system, a run consists of an incident ion normally and randomly entering a new ‘undamaged’ MWCNT. For better accuracy, statistics need to be 1×10^5 in simulating the data in this work.

The present static MC simulation programs include the first and the second steps. At the first step, we not only calculate ion-deposited energies but also record broken atomic bond, Frenkel pair, stopped ion and stopped recoil atom positions, in the MWCNT (or SWCNT). At the second step, we calculate the coordination defects and use a Kinchin–Pease model to estimate the number of vacancies produced in the MWCNT (or SWCNT). Therefore, we can describe the carbon nanotubes how to be disordered.

3 MC simulation results

The incident ion carrying E_0 above 50 keV easily penetrates through the MWCNT, while it becomes the penetrating ion with the $E_{penetrating}$ kinetic energy, so $E_0 - E_{penetrating}$ equals the ion-deposited energy in the MWCNT.

Figure 1 shows that under hundreds keV ^4He , ^{11}B , ^{12}C , ^{14}N , ^{20}Ne , ^{28}Si and ^{40}Ar ion irradiations, the average ion-deposited energy $E_0 - E_{penetrating}$ maximizes, while the ion mass has intermediate mass values, such as ^{11}B , ^{12}C and ^{14}N ion masses. Namely, the average $E_0 - E_{penetrating}$ maximizes for 50 keV ^{11}B , 100 keV ^{12}C and 200 keV ^{14}N ion irradiations of three shells. Note that for example, under hundreds keV ^4He (light), ^{20}Ne (intermediate) and ^{40}Ar (heavy) ion irradiations, the data (three shells) in Fig. 1 are about three times those (one shell) in Fig. 3.

As derived in Sect. 4 and in Fig. 2, the average ion-deposited energy $E_0 - E_{penetrating}$ can be compared with the ion-normalized energy $4EMm/(M + m)^2$ as follows: (A) The energy E is the ^{12}C ion-normalized energy, and it equals the ^{12}C ion-deposited energy. (B) The ion-normalized energy $4EMm/(M + m)^2$ maximizes, while the ion mass has ^{12}C mass value. (C) The $E_0 - E_{penetrating}$ curve approximates the $4EMm/(M + m)^2$ one, at 50 (circles), 100 (triangles) or 200 keV (squares) incident energies.

In order to simply study ion-induced damage of carbon nanotubes, we focus noble gas ion irradiations of the SWCNT. Figure 3 shows that the average ion-deposited energy $E_0 - E_{penetrating}$ maximizes, while its mass has an intermediate mass (^{20}Ne) value, under hundreds keV ^4He (light), ^{20}Ne (intermediate) and ^{40}Ar (heavy) ion irradiations of one shell. Correspondently, Fig. 4 shows that the average coordination defect number maximizes, while its mass has an intermediate mass (^{20}Ne) value, under hundreds keV ^4He , ^{20}Ne and ^{40}Ar ion irradiations of one shell. We derive an ion-deposited energy formula to analyze

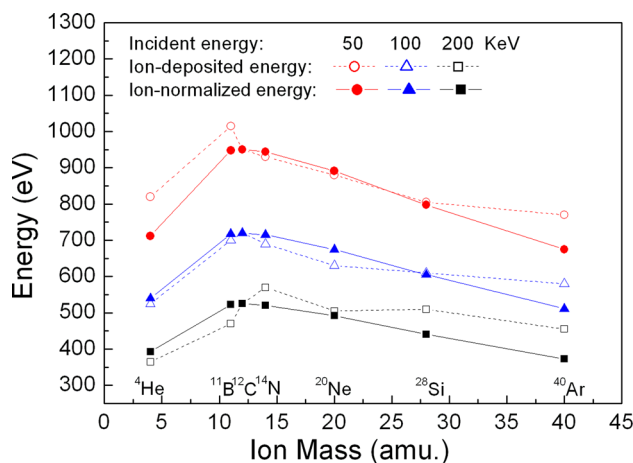


Fig. 2 Average ion-deposited energy $E_0 - E_{penetrating}$ (*open*) and the ion-normalized energy $4EMm/(M + m)^2$ (*solid*) as functions of the ion mass for ^4He , ^{11}B , ^{12}C , ^{14}N , ^{20}Ne , ^{28}Si and ^{40}Ar ion irradiations of a MWCNT composed of (10, 10), (15, 15) and (20, 20) SWCNTs, at 50 (circles), 100 (triangles) and 200 keV (squares) incident energies. Here, the $4EMm/(M + m)^2$ curve (*solid*) is derived from formula (8), and the $E_0 - E_{penetrating}$ one (*open*) comes from Fig. 1

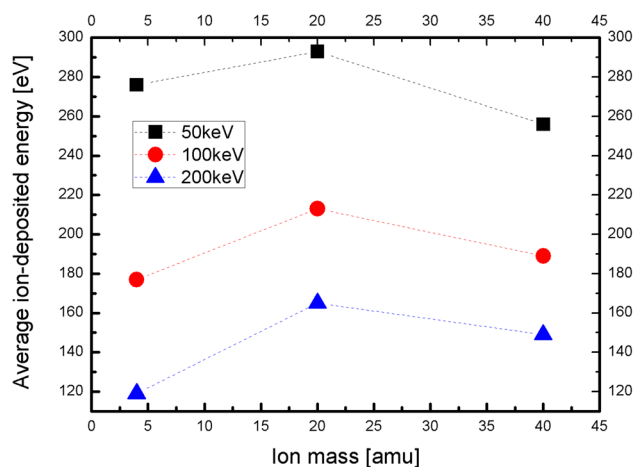


Fig. 3 Average ion-deposited energy $E_0 - E_{penetrating}$ as a function of the ion mass for ^4He , ^{20}Ne and ^{40}Ar ion irradiations of the SWCNT (20, 20), while incident energies $E_0 = 50, 100, 200$ keV

these maximum phenomena in Sect. 4. The Ar ion-induced defects are basic data in the MD results [7–11], so the ^{40}Ar ones are given in our MC results; as further studies, ^4He , ^{20}Ne and ^{40}Ar ion-induced defects are also given in our MC results, in Sect. 5, as comparison.

4 Derivation of formulas of the ion-deposited energies

As analyzed in Sect. 1, energetic ions and atoms can be seen as particles with nuclear point charge and nuclear point mass. Figure 5 describes the energetic ion how to

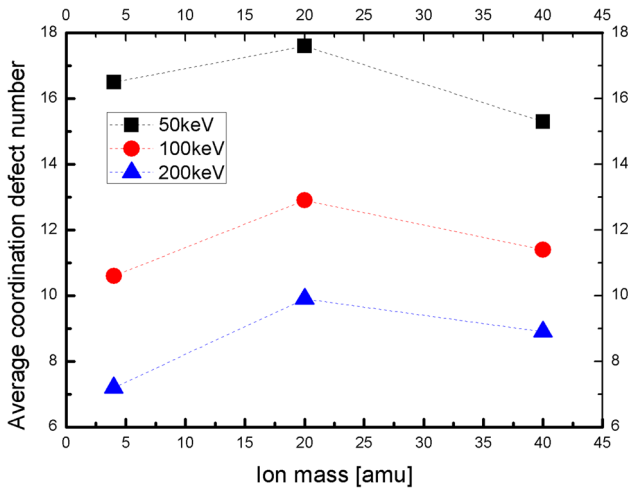


Fig. 4 Average coordination defect numbers as a function of ion mass for ⁴He (light), ²⁰Ne (intermediate) and ⁴⁰Ar (heavy) ion irradiations of the SWCNT (20, 20), while incident energies $E_0 = 50, 100, 200$ keV

collide with an atom, in the interaction potentials produced by nuclear point charges, in the center of mass system. In the interaction potentials, we can define the normal distance p between initial kinetic directions of the ion and an atom, to be the impact parameter; then we can define the θ angle between initial and final kinetic directions of the ion, to be the ion-scattered angle. Namely, the p impact parameter and then the θ ion-scattered angle necessarily exist in the interaction potentials of nuclear point charges. Therefore, the cross-sectional σ ($\sigma = \pi p^2$) effects suggested by Krasheninnikov et al. belong to the nuclear point charge effects.

In our present static MC simulation program, recoil atoms can be distinguished into two kinds, i.e., primary

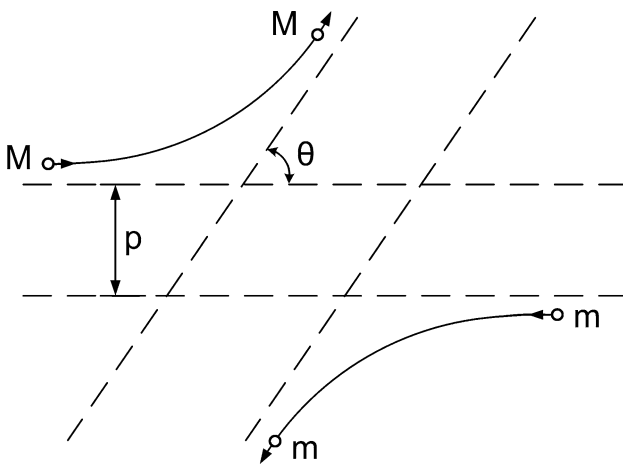


Fig. 5 Trajectories of the energetic ion and an atom in the interaction potentials of nuclear point charges, in the center of mass system. Here, M and m are nuclear point masses of the ion and an atom, p is the impact parameter, and θ is the ion-scattered angle

knock-on atom (PKA) and secondary knock-on atom (SKA) [22]. The PKA is the recoil atom produced by direct collision with an incident ion. The SKA is the recoil atom produced by other recoil atoms. For the incident ion carrying the E_0 incident energy, at $i + 1$ th collision between it and a lattice atom, the ion-transferred energy is defined to be the partial ion-deposited energy, i.e., $\Delta E_{i+1, \text{deposited}}$. The carbon atom displacement threshold energy T_d is anisotropic, and it may depend on the system geometry, etc. [9]. It is smaller in sp^2 -bonded carbon ($15 \rightarrow 20$ eV) than in diamond-like structures ($30 \rightarrow 48$ eV). Here, for computational convenience, T_d is assumed, on the average, to equal 28 eV energy.

At $i + 1$ th collision, we derive

$$E_i = E_{i+1} + \Delta E_{i+1, \text{deposited}} \tag{1}$$

where E_i and E_{i+1} are initial and final ion kinetic energies at $i + 1$ th collision.

In n collisions, we derive

$$E_0 = E_n + \sum_{i=0}^{n-1} \Delta E_{i+1, \text{deposited}} \tag{2}$$

where $n = 1, 2, \dots, \infty$ and E_n is the final ion kinetic energy in n collisions.

Based on energy and momentum conservations, at $i + 1$ th collision, we derive

$$E_i = E_{i+1} + \Delta E_{i+1, \text{deposited}} = E_{i+1} + E_i \gamma(M, m, \theta_{i+1}) \tag{3}$$

Based on energy and momentum conservations, in n collisions, we derive

$$E_0 = E_n + \sum_{i=0}^{n-1} E_i \gamma(M, m, \theta_{i+1}) \tag{4}$$

where $\gamma(M, m, \theta_{i+1})$ is transferred factor, θ_{i+1} is the ion-scattered angle in the center of mass system and M and m are ion and atom point masses.

For binary interactions, transferred factor $\gamma(M, m, \theta_{i+1})$ is classical [2, 12–22], that is,

$$\gamma(M, m, \theta_{i+1}) = (4Mm / (M + m)^2) \sin^2(\theta_{i+1} / 2) \tag{5}$$

Combing (4) and (5), we derive

$$E_0 = E_n + (4Mm / (M + m)^2) \sum_{i=0}^{n-1} E_i \sin^2(\theta_{i+1} / 2) \tag{6}$$

For a thin-walled carbon nanotube, if the incident energy is high enough, the incident ion carrying E_0 easily becomes the penetrating ion with the $E_n = E_{\text{penetrating}}$ kinetic energy. Thus, formula (6) becomes

$$E_0 = E_{\text{penetrating}} + (4Mm / (M + m)^2) \sum_{i=0}^{n-1} E_i \sin^2(\theta_{i+1} / 2) \tag{7}$$

where, evidently, $E_0 - E_{\text{penetrating}}$ equals the ion-deposited energy, i.e., $(4Mm/(M + m)^2) \sum_{i=0}^{n-1} E_i \sin^2(\theta_{i+1}/2)$.

For the MWCNT composed of (10, 10), (15, 15) and (20, 20) SWCNTs, irradiated by hundreds keV ions, our present simulations find $\sin^2(\theta_{i+1}/2) \ll 1$, i.e., $(\theta_{i+1}/2 \rightarrow 0)$ as $E_{i+1} \gg 1$ keV. For example, $\sin^2(\theta_{\text{average}}/2) \approx 0.00337$ for 50 keV ^{11}B ion irradiation of the MWCNT, where θ_{average} is the average ion-scattering angle in the center of mass system. Therefore, for the irradiated MWCNT, because $\gamma(M, m, \theta_{i+1}) \rightarrow 0$ as $(\theta_{i+1}/2) \rightarrow 0$, $E_0 \approx E_1 \approx \dots \approx E_i \approx E_{i+1} \approx \dots \approx E_n = E_{\text{penetrating}}$ in (7). Namely, the hundreds keV incident ion easily and swiftly penetrates through the thin-walled carbon nanotube, while in this tube, the ion-deposited energy \ll its incident energy. Our present simulations also find, for example, that on the average, an incident 50 keV ^{11}B ion produces about eight PKAs, for the MWCNT.

Based on above analysis, in (7) for the MWCNT irradiated by hundreds keV ions, if the $4Mm/(M + m)^2$ effects, i.e., the nuclear point mass effects, dominate over the angle-correlated energy $\sum_{i=0}^{n-1} E_i \sin^2(\theta_{i+1}/2)$ effects, in Fig. 1 the ion-deposited energy $E_0 - E_{\text{penetrating}}$ has a maximum, while the ion mass equals an intermediate mass value, such as ^{11}B , ^{12}C or ^{14}N ion masses.

As pointed out by a reviewer, would it be possible (or useful) to include in Fig. 2 the analytic mass effect ideal result, e.g., the $4EMm/(M + m)^2$ curve. The function $4X/(1 + X)^2$ with $X = m/M$ has a maximum at $X = 1$ (i.e., $m = M = ^{12}\text{C}$), the offset can be fixed by E , and it helps in understanding the role of the simulation with respect to the simple analytic result. Thus, formula (7) becomes formula (8), that is,

$$E_0 - E_{\text{penetrating}} \cong 4EMm/(M + m)^2 \tag{8}$$

Indeed, in Fig. 2 the $E_0 - E_{\text{penetrating}}$ curve approximates the $4EMm/(M + m)^2$ one, at 50 (circles), 100 (triangles) or 200 keV (squares) incident energies.

5 MD and MC simulation result comparisons

The MD simulations have works, such as (1) formation of ion-irradiation-induced atomic-scale defects on walls of carbon nanotubes [7], (2) carbon nanotubes as masks against ion irradiation [8], (3) ion ranges and irradiation-induced defects in multi-walled carbon nanotubes [10] and (4) relative abundance of single and double vacancies in irradiated single-walled carbon nanotubes [11]. Comparisons between the MD and the MC simulation results are as follows.

From SWCNT or MWCNT damage studies (1) in the MD simulations [7–11, 23], under keV-noble ion irradiations,

the cross-sectional σ for the defect production increases from light to heavy ions, as the ion nuclear charge Ze increases (Z is atomic number of the ion, and e is the charge on a proton.). Correspondently, the coordination defect number increases from light to heavy ions. Namely, the cross-sectional σ effects dominate the tube damage. However, in our MC simulations, under hundreds keV-noble ion irradiations, the ion-deposited energy $E_0 - E_{\text{penetrating}}$ maximizes, while its mass has an intermediate mass (^{20}Ne) value (Fig. 2). Correspondently, the coordination defect number maximizes, while its mass has an intermediate mass (^{20}Ne) value (Fig. 3). Note that a Ne ion has the most $4Mm/(M + m)^2$ value in He, Ne, Ar, Kr and Xe ions. Namely, the $4Mm/(M + m)^2$ effects dominate the tube damage, as analyzed by formula (7). (2) In the MD simulations, under 1 keV Ar ion irradiation, the coordination defect number equals 15 for one shell, while it equals 45 for three shells (Fig. 2 of [10]). However, in our MC simulations, under 100 keV ^{40}Ar ion irradiation, the coordination defect number equals 11 for one shell (Fig. 3), while it equals 35 for three shells. (3) In the MD simulations, under 1 keV Ar ion irradiation, the number of total vacancies equals 2.4 for (10, 10) SWCNT (Fig. 2 of [7]), and the number of single vacancies equals 1, while that of double ones equals 0.5 for (8, 8) SWCNT (Fig. 1 of [11]). However, in our MC simulations, under 100 keV ^{40}Ar ion irradiation, the number of total vacancies equals 1.8 for (20, 20) SWCNT. (4) As further studies, in our MC simulations, the $4Mm/(M + m)^2$ effects dominate coordination defects and vacancies. For example, for the 100 keV ion-irradiated (20, 20) SWCNT, the ^4He -induced coordination defect number equals 10, the ^{20}Ne one equals 13, and ^{40}Ar one equals 11. Also in this shell, the ^4He -induced number of total vacancies equals 1.6, the ^{20}Ne one equals 2.1, and the ^{40}Ar one equals 1.8.

From SWCNT or MWCNT stopping studies, (1) What is the maximum energy E_{th} of incident Ar ions for the MWCNT with an outer diameter at which no damage is created in the metal layer below the MWCNT? (Fig. 1 of [8]). In the MD simulations, the number of recoils (both Ar and C atoms) per 100 ions equals 0 at $E_{\text{th}} = 0.2$ keV for two shells or at $E_{\text{th}} = 0.75$ keV for six shells (Fig. 2 of [8]). Thus, the MWCNT with tens of shells can easily stop energetic Ar ions with energies up to 10 keV. (2) Also in the MD simulations, it equals 100 at $E_i = 0.7$ keV for three shells or at $E_i = 1.3$ keV for five shells (Fig. 2 of [8]). Thus, the MD simulation results may imply that at $E_i - 1$ keV for three (or five) shells, incident Ar ions easily become penetrating ions. This is why at $E_i = E_0 = 50, 100, 200$ keV for one (or three) shells, incident ^{40}Ar ions easily become penetrating ions, in our MC simulations. (3) As further studies, our MC simulations show that under hundreds keV ^4He , ^{11}B , ^{12}C , ^{14}N , ^{20}Ne , ^{28}Si and ^{40}Ar ion

irradiations, these incident ions easily and swiftly penetrate through the thin-walled carbon nanotubes, because in these tubes, the ion-deposited energies are much less than, i.e., \ll , their incident energies (Figs. 1, 2).

6 Summary

We have calculated the deposited energies of various energetic ions in carbon nanotubes, to study the nuclear point mass effects, with the help of a static MC simulation program. We derive an ion-deposited energy formula (7) for the thin-walled carbon nanotube. In this formula, the $E_0 - E_{\text{penetrating}}$ ion-deposited energy equals the product of the $4Mm/(M+m)^2$ ratio and the $\sum_{i=0}^{n-1} E_i \sin^2(\theta_{i+1}/2)$ angle-correlated energy. It should be emphasized here that the hundreds keV incident ion easily and swiftly penetrates through the thin-walled carbon nanotube, while in this tube, the ion-deposited energy \ll its incident energy (Fig. 1). For foundational mass-dependent collisions, the $4Mm/(M+m)^2$ effects mean each collision between one and another point mass particles along a straight line, if one and another point masses equal M and m , respectively.

We show that as a result of the nuclear point mass effects, i.e., the $4Mm/(M+m)^2$ effects, at the same incident energy, the ion-deposited energy maximizes, while its mass has intermediate mass values, such as ^{11}B , ^{12}C and ^{14}N ion masses, under hundreds keV ^4He , ^{11}B , ^{12}C , ^{14}N , ^{20}Ne , ^{28}Si and ^{40}Ar ion irradiations of three shells. We also show that at the same incident energy, the coordination defect number maximizes, while its mass has an intermediate mass (^{20}Ne) value, under hundreds keV ^4He , ^{20}Ne and ^{40}Ar ion irradiations of one shell. This is because the $4Mm/(M+m)^2$ effects, i.e., the nuclear point mass effects, dominate over the $\sum_{i=0}^{n-1} E_i \sin^2(\theta_{i+1}/2)$ effects.

As pointed out by a reviewer, would it be possible (or useful) to include in Fig. 2 the analytic mass effect ideal result, e.g., the $4EMm/(M+m)^2$ curve. Indeed, in Fig. 2 the $E_0 - E_{\text{penetrating}}$ curve approximates the $4EMm/(M+m)^2$ one, at 50 (circles), 100 (triangles) or 200 keV (squares) incident energies.

Acknowledgments This work was supported by National Basic Research Program of China (973 Program) No. 2010CB832903 and National Natural Science Foundation of China No. 11375251 and No 11175235.

References

1. P. Sigmund, *Particle Penetration and Radiation Effects: General Aspects and Stopping of Point Charge* (Springer, Berlin, 2006)
2. P. Sigmund, A. Fettouhi, A. Schinner, Nucl. Instrum. Methods B **209**, 19 (2003)
3. M.T. Robinson et al., Phys. Rev. **132**, 2385 (1963)
4. L.P. Zheng et al., Nucl. Instrum. Methods B **269**, 1472 (2011)
5. J.P. Biersack, L.G. Haggmark, Nucl. Instrum. Methods **174**, 257 (1980)
6. P. Sigmund, Nucl. Instrum. Methods **B18**, 375 (1987)
7. A.V. Krasheninnikov, K. Nordlund, J. Keinonen, Phys. Rev. B **63**, 245405 (2001)
8. A.V. Krasheninnikov, K. Nordlund, J. Keinonen, Appl. Phys. Lett. **81**, 1101 (2002)
9. A.V. Krasheninnikov, K. Nordlund, J. Appl. Phys. **107**, 071301 (2010)
10. J. Pomoell, A.V. Krasheninnikov, K. Nordlund, J. Keinonen, J. Appl. Phys. **96**, 2864 (2004)
11. A. Tolvanen, J. Kotakoski, A.V. Krasheninnikov, K. Nordlund, Appl. Phys. Lett. **91**, 173109 (2007)
12. L.P. Zheng, Z.Y. Zhu, Y. Li, D.Z. Zhu, H.H. Xia, J. Phys. Chem. C **112**, 15204 (2008)
13. J.F. Ziegler, J.P. Biersack, U. Littmark, *The Stopping and Range of Ions in Matter* (Pergamon, New York, 1985)
14. R. Smith (ed.), *Atomic & Ion Collisions in Solids and at Surfaces: Theory, Simulation and Applications* (Cambridge University Press, Cambridge, 1997)
15. P.M. Echenique, R.M. Nieminen, J.C. Ashley, R.H. Ritchie, Phys. Rev. A **33**, 897 (1986)
16. P. Stampfli, Nucl. Instrum. Methods B **107**, 138 (1996)
17. G. Schiwietz, Nucl. Instrum. Methods B **175–177**, 1 (2001)
18. A.E. Volkov, V.A. Borodin, Nucl. Instrum. Methods B **107**, 172 (1996)
19. L.P. Zheng, R.S. Li, X.Q. Xia, M.Y. Li, Appl. Phys. A **61**, 419 (1995)
20. L.P. Zheng, Y.G. Ma, J.G. Han, D.X. Li, X.R. Zhang, Phys. Lett. A **324**, 211 (2004)
21. P. Sigmund, Phys. Rev. **184**, 383 (1969)
22. L.P. Zheng, Nucl. Instrum. Methods B **142**, 30 (1998)
23. J. Pomoell, A.V. Krasheninnikov, K. Nordlund, Nucl. Instrum. Methods **B206**, 18 (2003)
24. L. Yan et al., Carbon **46**, 376 (2008)
25. L. Yan et al., Carbon **49**, 2141 (2011)
26. L. Yan et al., Diam. Relat. Mater. **17**, 365 (2008)